IJPST
Indonesian Journal of Pharmaceutical Science and Technology

Research Article
Vol.12. Suppl.2 (2025), 66-73
https://doi.org/10.24198/ijpst.v12s2.58912

Exploration of Anti-FABP3 Aptamer Conformation Using Coarse-Grained Molecular Dynamics Simulation

A S. Aathirah[1], Ari Hardianto[2,3] and Shabarni Gaffar[1,2,3*]
[1]Graduate School, Universitas Padjadjaran, Bandung, West Java, Indonesia
[2]Department of Chemistry, Faculty of Mathematics and Natural Sciences, Universitas Padjadjaran, Sumedang, West Java, Indonesia
[3]Research Center for Molecular Biotechnology and Bioinformatics, Universitas Padjadjaran, Bandung, West Java, Indonesia

Abstract
Aptamers have been extensively utilized in the development of diagnostic and therapeutic methodologies for a variety of diseases. Aptamer N13, obtained through the SELEX process in previous research, has been identified as an anti-FABP3 ssDNA aptamer to enhance diagnostic techniques for myocardial infarction. This study provides an in-depth examination of the conformation and structural dynamics of aptamer N13 using in silico methods. These include secondary structure prediction via DNAfold, 3D structures modeling through RNAComposer, and coarse-grained molecular dynamics (MD) simulations with SIRAH AMBER. The 83 μs MD simulation results reveal that the predicted conformation generally struggles to maintain stability, as indicated by the RMSD values and their fluctuations. However, residues 1-50 demonstrate relatively stable conformations, particularly beyond the 40 μs point in the simulation. In contrast, residues 51-90, constituting the free end, exhibit persistent conformational instability. This instability is likely attributable to their single-stranded and free nature compared to the other regions characterized by loops that confer greater stability. Our findings suggest that the predicted conformation from existing tools does not yet provide the most stable reference structure, necessitating further exploration through extended molecular dynamics simulations.

Keywords: Aptamer, Anti-FABP3, Conformation, Molecular Dynamic Simulation

Article History:
Submitted 6 November 2024
Revised 13 January 2025
Accepted 17 January 2025
Published 12 February 2025

*Corresponding author:
shabarni.gaffar@unpad.ac.id

Citation:
Aathirah, A. S., Hardianto A., Gaffar, A. Exploration of Anti-FABP3 Aptamer Conformation Using Coarse-Grained Molecular Dynamics Simulation. Indonesian Journal of Pharmaceutical Science and Technology. 2025: Vol.12 Suppl.2: 66-73

Eksplorasi Konformasi Aptamer Anti-FABP3 Menggunakan Simulasi Dinamika Molekuler Secara *Coarse-Grain*

Abstrak
Aptamer telah banyak digunakan dalam pengembangan metodologi diagnostik dan terapeutik untuk berbagai penyakit. Aptamer N13, yang diperoleh melalui proses SELEX dalam penelitian sebelumnya, telah diidentifikasi sebagai aptamer ssDNA anti-FABP3 untuk meningkatkan teknik diagnostik infark miokard. Studi ini memberikan observasi mendalam tentang konformasi dan dinamika struktural aptamer N13 menggunakan metode in silico. Metode ini termasuk prediksi struktur sekunder melalui DNAfold, pemodelan struktur 3D melalui RNAComposer, dan simulasi dinamika molekuler (MD) secara coarse grain dengan SIRAH AMBER. Hasil simulasi MD selama 83 μs menunjukkan bahwa konformasi yang diprediksi umumnya kesulitan untuk mempertahankan stabilitas, didukung oleh nilai RMSD dan fluktuasinya yang tinggi. Namun, residu 1-50 menunjukkan konformasi yang relatif stabil, terutama pada simulasi setelah 40 μs. Sebaliknya, residu 51-90, yang membentuk ujung bebas, menunjukkan ketidakstabilan konformasi secara konstan. Ketidakstabilan ini kemungkinan disebabkan oleh sifat bebas dari untai tunggal mereka dibandingkan dengan wilayah lain yang ditandai oleh loop yang memberikan stabilitas lebih besar. Temuan kami menunjukkan bahwa konformasi yang diprediksi dari alat bioinformatika yang ada belum menyediakan referensi struktur yang paling stabil, sehingga memerlukan eksplorasi lebih lanjut melalui simulasi dinamika molekuler yang panjang.

Kata Kunci: Aptamer, Anti-FABP3, Konformasi, Simulasi Dinamika Molekuler

1. Introduction

Aptamers have been extensively developed to detect or diagnose various diseases caused by bacteria, viruses, and metabolic diseases that can be detected through specific proteins.[1–3] Aptamers are considered alternatives to antibodies (monoclonal, polyclonal, scFv, Fab) in diagnostic and therapeutic applications.[4] Aptamers are oligonucleotides in the form of ssRNA/ssDNA (single-stranded RNA, DNA) that bind to specific targets with significant dependency and exclusivity due to their specific structural characteristics.[5] Aptamers offer several advantages as alternatives in diagnostic and therapeutic applications compared to antibodies. These include unlimited/long shelf life, small size that facilitates tissue penetration, high specificity and affinity, high stability against temperature and pH changes, low immunogenicity, the ability for diverse modifications by various molecules, and relatively lower production costs.[4]

Aptamers are traditionally generated through a process known as SELEX (Systematic Evolution of Ligands by Exponential Enrichment). This procedure for identifying aptamers typically involves several stages: library creation, target incubation, selection, and aptamer amplification.[6,7] Despite its widespread use, conventional SELEX methods face several significant limitations, including the extended duration required for aptamer development, which can span from several weeks to months for a single aptamer, and a relatively low success rate.[8]

In recent years, numerous bioinformatics tools have emerged designed to aid and enhance the selection and optimization processes for aptamers. These tools are integrated into the aptamer identification process to expedite development time, reduce research costs, and provide more precise test analyses. Incorporating bioinformatics significantly improves the likelihood of obtaining aptamers with optimal characteristics and high affinity for their target molecules. This integration of advanced bioinformatics into the SELEX process marks a significant advancement, enabling the generation of high-quality aptamers more efficiently and cost-effectively. This progress underscores the importance of continual technological innovation in aptamer research and development.

Molecular dynamics (MD) simulations represent a highly effective methodology for examining biological molecules' molecular structure, interactions, and dynamics at a detailed molecular level.[9,10] However, due to computational constraints associated with MD simulations, coarse-grain (CG) models have been extensively utilized to investigate DNA structure conformation and folding mechanisms. In studies related to conformational exploration, CG models are preferred over all-atom models because they are more efficient in exploring different conformations. This is due to their ability to reduce the number of degrees of freedom.[11] CG modeling simplifies complex atomic systems by averaging non-essential degrees of freedom, enabling a more comprehensive exploration of conformational landscapes.[12,13]

Kakoti and Goswami (2017), conducted a comprehensive screening of aptamer candidates capable of recognizing Fatty Acid-Binding Protein 3 (FABP3), a potential biomarker for myocardial injury, using the SELEX method.[14] Among the screened candidates, aptamer N13 emerged as one of the most promising. This study aims to validate the structures obtained from prediction tools using CG-models molecular dynamics. This conformational exploration of the 3D structure of aptamer N13 will help us strengthen our understanding of their native dynamics throughout the simulation since the experimental structure has yet to be obtained. The rigorous analysis of the aptamer's structural dynamics will highlight its potential stability and suitability in practical diagnostic applications. This exploration is pivotal for advancing aptamer N13 as a viable and efficient biomarker for early myocardial injury detection, paving the way for more effective heart attack diagnostics.

2. Materials and Methods

2.1. Tools

From the preparation until the coarse-grain molecular dynamic simulation for 1 to 50 μs was performed on an Intel® Xeon® CPU E5-2670 v3 with 14 cores and 28 threads, and for simulation lengths from 51 to 83 μs on an Intel® Xeon® CPU E5-2670 v3 with 16 cores and 32 threads, both using Amber22.

2.2. Materials

The parent aptamer utilized in this study pertains to the specific ssDNA aptamer for FABP3, identified in the prior research conducted by Kakoti and Goswami (2017), designated as N13.[14] This particular aptamer comprised 90 nucleotides and was obtained through the SELEX method. The N13 aptamer sequence is provided in Table 1.

2.3. Methods

2.3.1. 2D and 3D Structure Predictions of N13 Aptamer

The secondary and tertiary structure predictions of aptamer N13 followed the protocol outlined in the reference study.[14] Initially, the secondary structure was

Tabel 1. Nucleotide Sequence of N13 Aptamer.[14]

Name	Nucleotides Sequence	Length
N13	5'CACCTAATACGACTCACTATAGCGGATCCGAAGGGGGCGCGAGGTGTAAGG-GTGTGGGGTGGTGGGTGGGCCTGGCTCGAACAAGCTTGC3'	90 nt

predicted by inputting the N13 sequence into the Mfold web server (DNA fold, http://www.unafold.org/).[15] For the 3D structure, the N13 sequence, with thymine (T) bases replaced by uracil (U), along with the dot-bracket notation of the secondary structure, was inputted into the RNA Composer webserver (https://rnacomposer.cs.put.poznan.pl).[16,17] The generated 3D structure was saved in PDB format for further use. Further preparation of the 3D N13 structure involved converting the RNA sequence back to ssDNA by replacing each uracil (U) base with thymine (T). Additionally, the phosphate atom at the first base was removed, and the sugar in all bases was changed from ribose to deoxyribose.

2.3.2. Coarse-grained Molecular Dynamic Simulation

MD simulations for simulation lengths from 1 to 50 μs were performed on an Intel® Xeon® CPU E5-2670 v3 with 14 cores and 28 threads, and for simulation lengths from 51 to 83 μs on an Intel® Xeon® CPU E5-2670 v3 with 16 cores and 32 threads, both using Amber22. The atomic structure of 90 nt ssDNA was mapped into a CG representation. The CG structure was then inputted into the LEaP program, with the force field used being SIRAH and the explicit solvent being WatFour (WT4). Solvent, counterions, and 0.15 M NaCl were added to provide hydration and neutralize the N13 charge. The input values for NaW and ClW were 219 and 130, respectively. Subsequently, energy minimization, equilibration (NPT), and production were performed. These procedures followed Tutorial 2. SIRAH force field in AMBER for coarse-grained molecular dynamics simulation of DNA molecules in explicit solution.[18,19]

2.3.3. Visualization, Backmapping, and RMSD Analysis

The visualization of molecular dynamics simulation results is carried out using VMD (Visualizer Molecular Dynamics) software. Molecules are added by selecting files with the .nc extension and adding the PRMTOP file after adding all the NC files to be visualized. Next, the source input file sirah_vmdtk.tcl is used to display the visual representation in the form of sirah_nucleic. Then, backmapping is performed using the command sirah_backmap, transforming the coarse-grained molecular dynamics simulation results back to all atoms model through this backmapping stage. The backmap results are obtained in PDB file format and used for the analysis. RMSD analysis is performed using the RMSD Trajectory Tool, and the RMSD Plot and Heatmap Plot from the molecular dynamics simulation is obtained.

3. Result

According to the secondary structure predicted using DNAfold, as illustrated in Figure 1A, the region encompassing residues 1 to 55 forms three stems

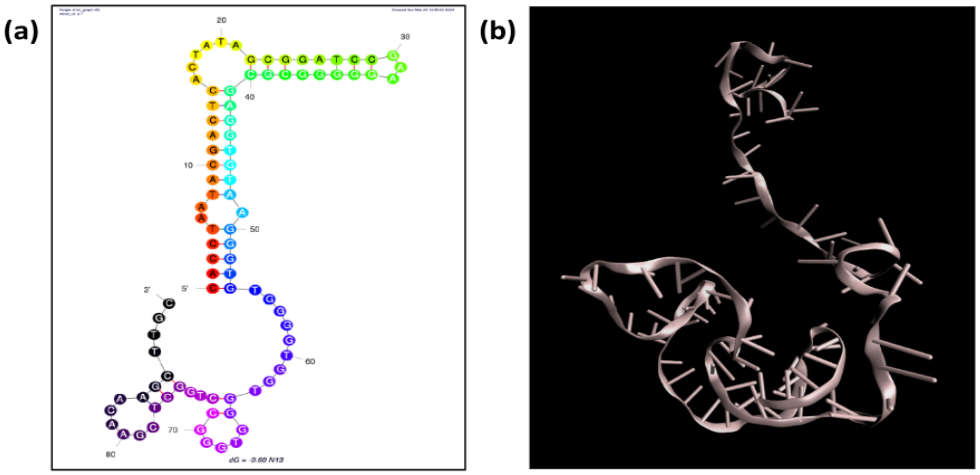

Figure 1. (a) 2D structure of N13 by using DNAfold, a DNA secondary structure prediction tool, (b) 3D structure of N13 by using RNA Composer and then converted into a DNA sequence.

and three loops. In contrast, the region spanning residues 56 to 90 features a free end with two loops. In DNA aptamers' secondary structures, Watson-Crick base pairing typically occurs, where nucleotide bases complement each other, forming loops and stems within the aptamer structure, while non-complementary bases result in free ends.[20] Fundamentally, the secondary structure arises from nucleotide base pairing within the aptamer, facilitating interactions with its target. The Mfold web server is a preeminent tool widely used for predicting the secondary structures of aptamers (ssDNA/RNA). This prediction relies on minimum free energy and ΔG as the core algorithm, enabling the specific folding of base pairs.[15] Notably, the predicted ΔG for the secondary structure of the N13 aptamer is -9.63.

The predicted three-dimensional structure, which underwent coarse-grained molecular dynamics analysis and subsequent backmapping, serves as the reference (Figure 1B) for further examination, focusing on Root Mean Square Deviation (RMSD). The stability differences between these two regions will be analyzed and discussed further. RNA algorithms are predominantly utilized in nucleic acid 3D structure prediction, with RNAComposer standing out as one of the most prominent and widely adopted web servers.[21] The conversion of DNA structural information into RNA structures is considered reliable. In silico methodologies have demonstrated that the predicted structures are remarkably similar to experimental data, highlighted by the formation of hairpins and the accurate structuring of small fragments.[5]

The utilization of RNAComposer as a primary tool for predicting 3D structures stems from its significant advantages, including brief computation time, high efficiency, and ease of access to high-resolution RNA structural models. Furthermore, structural refinement through several rapid stages, such as adjusting the number of atoms, results in highly optimized structures.[16,22,23] Given the output in RNA format, a crucial subsequent step was converting this structure to DNA molecules. Hence, the four common steps in predicting the 3D structure of ssDNA aptamers were: (i) predicting the 2D structure using Mfold, (ii) predicting the 3D structure with RNAComposer, (iii) modifying and converting the RNA structure to DNA, and (iv) performing energy minimization.[21]

Following an 83 μs coarse-grained molecular dynamics simulation, Figure 2A illustrated that the conformation of aptamer N13 continuously changed as it sought stability within its native environment. These movements were depicted through the color progression in the timestep trajectory, transitioning from red to blue, and the trajectory displayed excludes hydrogen atoms (noh). Some observed movements were back-and-forth motions, potentially indicative of the inherent activity of aptamer N13. However, most movements appeared random and lacked a distinct pattern, which may reflect the aptamer's efforts to attain a stable conformation or represent natural, expected motions. Furthermore, the RMSD analysis (Figure 2B) using the initial structure, which is the structure obtained from the prediction tool, as a reference indicated progressively increasing values as the conformation evolves throughout the simulation, with the highest value reaching 25.78 Å, the lowest value reaching 2.75 Å, and an average of 19.86 Å (standard deviation 3.37 Å). RMSD values represent the average distance between atoms along the backbone for each frame in the simulation trajectory, commonly used to measure and map conformational

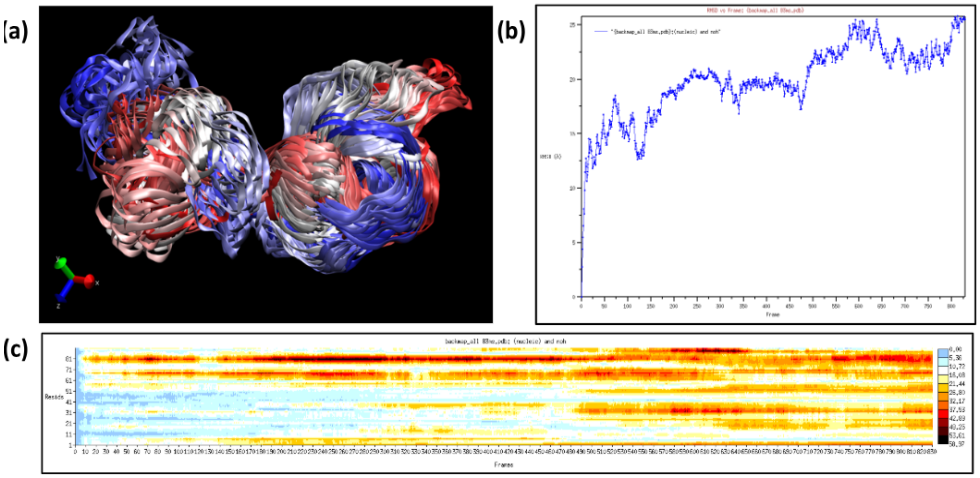

Figure 2. **(a)** Conformation alignment (backbone only) all residue from 1 to 83 μs, every 1 μs contains 10 frames, frame 1 (initial structure) as the reference, **(b)** RMSD Plot all residue from 1 to 83 μs, frame 1 as the reference, **(c)** Heatmap Plot all residue from 1 to 83 μs, frame 1 as the reference.

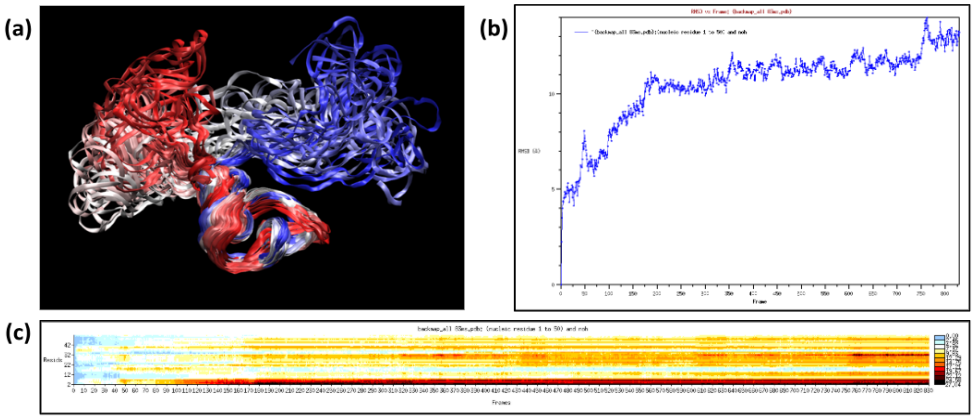

Figure 3. (a) Conformation alignment (backbone only) residue 1-50 from 1 to 83 µs, every 1 µs contains 10 frames, frame 1 (initial structure) as the reference, **(b)** RMSD Plot residue 1-50 from 1 to 83 µs, frame 1 as the reference, **(c)** Heatmap Plot residue 1-50 from 1 to 83 µs, frame 1 as the reference.

changes within a structure.[24] RMSD generally indicates structural rigidity; thus, side chain interactions, such as hydrogen bonding, can significantly differ even if two structures seem similar.[25] The persistently high and increasing RMSD values suggested that the current conformation remains unstable and misaligned with its reference structure. However, the heatmap plot (Figure 2C) revealed a trend where residues 1 to 50 exhibit relative stability despite ongoing adjustments, while residues 51 to 90 persistently deviated from the initial reference conformation, indicating continuous movement.

Subsequently, we tried to align all conformations precisely to residues 1 to 50, as shown in Figure 3A. This indicated a specific movement converging towards a particular position to attain a relatively stable conformation. This was supported by the heatmap plot (Figure 3C) for residues 1 to 50, showing that although conformational changes occurred in this region throughout the simulation, the changes were not as contrasting and random as those observed in another area. Within this region, significant shifts were predominantly observed in residues 1 to 10, but these alterations specifically converged towards a stable and non-random final position. Despite this, the RMSD plot (Figure 3B) showed quite a contrasting change between the final conformation and the initial reference conformation. The RMSD score reached the highest value of 13.56 Å and the lowest value of 2.24 Å with an average value of 10.03 Å (standard deviation 2.15 Å) and relatively high fluctuation values continuously throughout the simulation. However, this does not necessarily conclude that the final conformation lacks sufficient stability. This is because the RMSD analysis employs the initial conformation as a reference, a predicted conformation that may not always represent the most stable or experimentally consistent conformation.

Upon conducting further analysis, we determined that the conformation of the aptamer began to stabilize at a simulation length of 40 µs, particularly for residues 1 to 50, as illustrated in Figure 4A. The RMSD plot, with the 40 µs conformation as a reference (Figure 4B), demonstrated that the gaps in RMSD values for each conformation began to narrow and tended to stabilize, as evidenced by the absence of significant RMSD

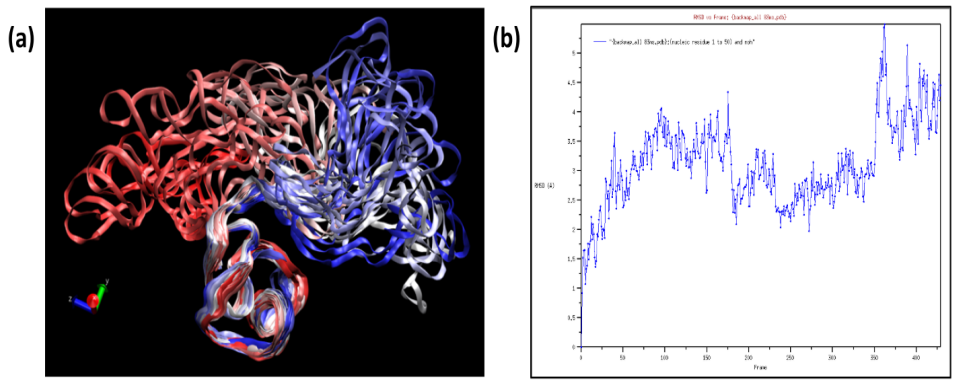

Figure 4. (a) Conformation alignment (backbone only) residue 1-50 from 40 to 83 µs, every 1 µs contains 10 frames, frame 400 (40 µs) as the reference, **(b)** RMSD Plot residue 1-50 from 40 to 83 µs, frame 400 as the reference.

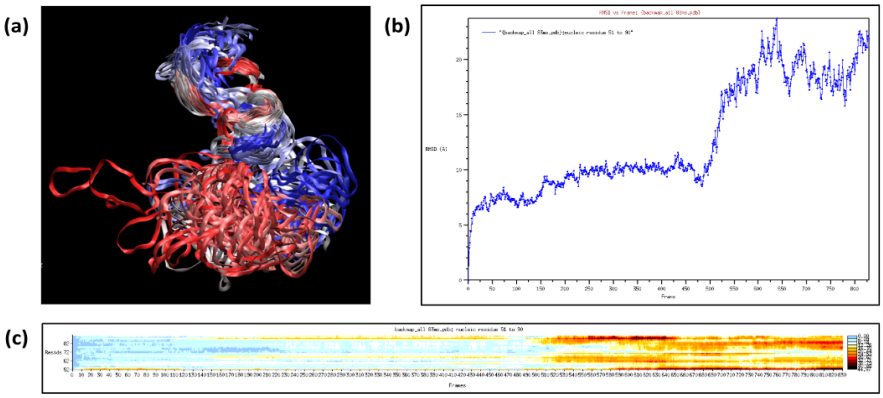

Figure 5. (a) Conformation alignment (backbone only) residue 51-90 from 1 to 83 µs, every 1 µs contains 10 frames, frame 1 (initial structure) as the reference, **(b)** RMSD Plot residue 51-90 from 1 to 83 µs, frame 1 as the reference, **(c)** Heatmap Plot residue 51-90 from 1 to 83 µs, frame 1 as the reference.

spikes throughout the remainder of the simulation. The RMSD graph indicates a notable decrease in RMSD values, with the highest recorded value at 5.49 Å and the lowest at 0.92 Å, averaging 3.11 Å (standard deviation 0.71 Å), showing relatively stable fluctuations consistently. At the 40 µs simulation mark, the conformation started to converge towards a more specific position, with less significant conformational changes occurring. It was probable that within the 40 to 83 µs simulation range, this region began to achieve stability and moved naturally according to its native characteristics.

In residues 51 to 90, a pervasive random movement did not converge to a single position (Figure 5). This may be due to its single-strand structure and its being a free end that tends to move quickly and is naturally unstable. Figure 5B illustrated a significant surge in RMSD values, peaking at 23.74 Å, with a minimum of 2.50 Å and an average of 12.75 Å (standard deviation 5.07 Å), using frame 1 as the reference. One critical factor affecting aptamer stability is hydrogen bonding.[26] There's quite a significant spike in the RMSD value at a simulation length of 49 µs, as also shown in Figure 5C, where residues 51-90 were generally relatively stable from the start of the simulation until around 49 µs, at which point a significant change in the conformation in that region begins to occur. An aptamer's reduction or diminished stability may be attributed to a decrease or insufficient formation of hydrogen bonds within the overall conformation.

4. Discussion

During the simulation, we did not consider the binding site since it has not been known yet. This simulation was conducted to ensure that the structures obtained from prediction tools are accurate and stable, knowing that no homolog or template structure could be used as a reference since this aptamer is not yet crystalized and only the sequence that has been published. However, through a comprehensive exploration of the aptamer N13 conformation, our analysis has determined that initial structures obtained from prediction tools do not serve as optimal references for experimental-based conformations.

This was evidenced by their suboptimal stability, as demonstrated by molecular dynamics simulations, and elevated RMSD fluctuation values. Although prolonged simulations beyond the 83 µs may continue to show conformational exploration and changes, these changes were expected to be minor. It was anticipated that stable conformations for these residues, exhibiting RMSD values < 2 Å, may be achieved with further simulations. This necessitates additional analysis to ascertain the role of these residues in the activity of aptamer N13. Sequence modifications in this region should be considered to enhance overall conformational stability. In summary, while aptamer N13 shows promise in stability within certain residue regions, extensive analysis and potential modifications are required to optimize its structural stability fully.

The three-dimensional structure of an aptamer, including its affinity and specificity, significantly relies on the derived secondary structure. Predominantly, structural predictions are based on sequence homology obtained from validated experimental databases. Typically, the 3D structure of an aptamer features folds comprising combinations of stems, hairpins, loops, pseudoknots, bulges, or G-quadruplexes. The (deoxy)ribose-phosphodiester backbone is a standard for evaluating the feasibility of the resultant structure, with six torsional angles facilitating the formation of various predicted secondary and tertiary structures of the aptamer.[27] Therefore, ensuring the predicted secondary structure is sufficiently accurate is crucial. Besides Watson-Crick base pairs, another typical interaction found in structures is the formation

of G-quadruplexes, which can also occur in the conformation of DNA aptamers. G-quadruplex formation plays a crucial role in the structural stability of DNA aptamers. Generally, G-quadruplex formation in aptamer structures arises due to the abundance of guanine in the DNA/RNA aptamer sequence. This formation consists of four guanines positioned at four parallel corners, each forming two hydrogen bonds with two neighboring guanines, thus creating G-tetrads. The presence of several G-tetrads is referred to as a G-quadruplex.[20] In this study, no G-quadruplex formation was found in the 3D structure of the N13 aptamer. This absence may contribute to the structural instability of this ssDNA, considering the relatively few hydrogen bonds formed.

The instability predominantly attributed to the region encompassing residues 51 to 90 could be mitigated through modifications, such as excising this region from the N13 aptamer sequence, while duly considering its role in binding and specificity towards the target. In the context of SELEX-derived aptamer optimization through modification, it is imperative to preserve the spatial integrity of the folded structure, as any alterations may impact the aptamer's affinity and specificity.[28] Typically, the binding site of an aptamer is located within the stem region of its structure. The interactions between the aptamer and its target generally include hydrogen bonds, electrostatic interactions, and van der Waals forces.[29,30] Consequently, modifications or conformational changes at the aptamer's binding site could influence its binding properties and affect its stability and specificity.

Based on a study by Auiewiriyanukul et al., stabilizing the conformation of a molecule can enhance its specificity in binding to its ligand.[31] This supports the importance of ensuring the conformational stability of a biomolecule that acts as a receptor or detector in its development for diagnostic applications to maintain or improve its specificity in recognizing its target. However, according to Warfield and Anderson, conformational changes at the binding site are sometimes necessary to optimize the binding ability of an aptamer to form a complex with its target. The presence of specific ions can also affect the affinity of an aptamer.[32] Therefore, the mechanism and binding properties of the N13 aptamer with FAB3 need to be further investigated to provide a deeper understanding of this matter.

5. Conclusion

Residues 1 to 50 of PTmer N13 exhibit a consistent conformational pattern, with movements converging towards a specific position. This region demonstrates significant conformational stability in simulations at 40 μs, indicated by a decrease in RMSD fluctuation values. Conversely, residues 51 to 90 illustrate a tendency for increased mobility, leading to continuous increases in RMSD values.

Acknowledgments

This research was funded by the Ministry of Education and Culture, Research and Technology, Indonesia, grant number 3018/UN6.3.1/PT.00/2023. We also thank the Research Center of Molecular Biotechnology and Bioinformatics at Universitas Padjadjaran and Noto Susanto Gultom from the Department of Physics, Faculty of Mathematics and Natural Sciences, Universitas Padjadjaran, for providing the computer facilities.

Conflict of Interest

The authors declare no conflicts of interest.

References

1. Li L, Li Q, Liao Z, Sun Y, Cheng Q, Song Y, et al. Magnetism-Resolved Separation and Fluorescence Quantification for Near-Simultaneous Detection of Multiple Pathogens. Anal Chem. 2018;90(15).
2. Ye H, Duan N, Gu H, Wang H, Wang Z. Fluorometric determination of lipopolysaccharides via changes of the graphene oxide-enhanced fluorescence polarization caused by truncated aptamers. Microchimica Acta. 2019;186(3).
3. Singh NK, Jain P, Das S, Goswami P. Dye coupled aptamer-captured enzyme catalyzed reaction for detection of pan malaria and p. Falciparum species in laboratory settings and instrument-free paper-based platform. Anal Chem. 2019;91(6).
4. Ahmadi S, Arab Z, Safarkhani M, Nasseri B, Rabiee M, Tahriri M, et al. Aptamer hybrid nanocomplexes as targeting components for antibiotic/gene delivery systems and diagnostics: A review. Vol. 15, International Journal of Nanomedicine. 2020.
5. Jeddi I, Saiz L. Three-dimensional modeling of single stranded DNA hairpins for aptamer-based biosensors. Sci Rep. 2017;7(1).
6. Srivastava S, Abraham PR, Mukhopadhyay S. Aptamers: An Emerging Tool for Diagnosis and Therapeutics in Tuberculosis. Vol. 11, Frontiers in Cellular and Infection Microbiology. 2021.
7. Ma X, Wang W, Chen X, Xia Y, Duan N, Wu S, et al. Selection, characterization and application of aptamers targeted to Aflatoxin B2. Food Control. 2015;47:545–51.
8. Zhuo Z, Yu Y, Wang M, Li J, Zhang Z, Liu J, et al. Recent advances in SELEX technology and aptamer applications in biomedicine. Vol. 18, International Journal of Molecular Sciences. 2017.
9. Nam KH. Molecular dynamics—from small molecules to macromolecules. Vol. 22, International Journal of Molecular Sciences. MDPI AG; 2021.
10. Buglak AA, Samokhvalov A V., Zherdev A V., Dzantiev BB. Methods and applications of in silico aptamer design and modeling. Vol. 21, International Journal of

Molecular Sciences. MDPI AG; 2020. p. 1–25.
11. Mustafa G, Nandekar PP, Yu X, Wade RC. On the application of the MARTINI coarse-grained model to immersion of a protein in a phospholipid bilayer. Journal of Chemical Physics. 2015;143(24).
12. ngólfsson HI, Lopez CA, Uusitalo JJ, de Jong DH, Gopal SM, Periole X, et al. The power of coarse graining in biomolecular simulations. Vol. 4, Wiley Interdisciplinary Reviews: Computational Molecular Science. 2014.
13. Dans PD, Walther J, Gómez H, Orozco M. Multiscale simulation of DNA. Vol. 37, Current Opinion in Structural Biology. 2016.
14. Kakoti A, Goswami P. Multifaceted analyses of the interactions between human heart type fatty acid binding protein and its specific aptamers. Biochim Biophys Acta Gen Subj. 2017;1861(1).
15. Zuker M. Mfold web server for nucleic acid folding and hybridization prediction. Nucleic Acids Res. 2003;31(13).
16. Popenda M, Szachniuk M, Antczak M, Purzycka KJ, Lukasiak P, Bartol N, et al. Automated 3D structure composition for large RNAs. Nucleic Acids Res. 2012;40(14).
17. Sarzynska J, Popenda M, Antczak M, Szachniuk M. RNA tertiary structure prediction using RNAComposer in CASP15. Proteins: Structure, Function and Bioinformatics. 2023;91(12).
18. Darré L, Machado MR, Brandner AF, González HC, Ferreira S, Pantano S. SIRAH: A structurally unbiased coarse-grained force field for proteins with aqueous solvation and long-range electrostatics. J Chem Theory Comput. 2015;11(2).
19. Darré L, MacHado MR, Dans PD, Herrera FE, Pantano S. Another coarse grain model for aqueous solvation: WAT FOUR? J Chem Theory Comput. 2010;6(12).
20. 20. Afanasyeva A, Nagao C, Mizuguchi K. Prediction of the secondary structure of short DNA aptamers. Biophys Physicobiol. 2019;16:287–94.
21. Ahmad NA, Mohamed Zulkifli R, Hussin H, Nadri MH. In silico approach for Post-SELEX DNA aptamers: A mini-review. J Mol Graph Model. 2021 Jun 1;105.
22. Purzycka KJ, Popenda M, Szachniuk M, Antczak M, Lukasiak P, Blazewicz J, et al. Automated 3D RNA structure prediction using the RNAComposer method for riboswitches1. In: Methods in Enzymology. Academic Press Inc.; 2015. p. 3–34.
23. 23. Biesiada M, Purzycka KJ, Szachniuk M, Blazewicz J, Adamiak RW. Automated RNA 3D structure prediction with RNA Composer. In: Methods in Molecular Biology. Humana Press Inc.; 2016. p. 199–215.
24. Fatima I, Ihsan H, Masoud MS, Kalsoom S, Aslam S, Rehman A, et al. Screening of drug candidates against Endothelin-1 to treat hypertension using computational based approaches: Molecular docking and dynamics simulation. Vol. 17, PLoS ONE. Public Library of Science; 2022.
25. Fowler NJ, Sljoka A, Williamson MP. A method for validating the accuracy of NMR protein structures. Nat Commun. 2020 Dec 1;11(1).
26. Xie YC, Eriksson LA, Zhang RB. Molecular dynamics study of the recognition of ATP by nucleic acid aptamers. Nucleic Acids Res. 2020 Jul 9;48(12):6471–80.
27. Krüger A, Zimbres FM, Kronenberger T, Wrenger C. Molecular modeling applied to nucleic acid-based molecule development. Vol. 8, Biomolecules. 2018.
28. Zhang N, Chen Z, Liu D, Jiang H, Zhang ZK, Lu A, et al. Structural biology for the molecular insight between aptamers and target proteins. Vol. 22, International Journal of Molecular Sciences. MDPI AG; 2021.
29. Cai S, Yan J, Xiong H, Liu Y, Peng D, Liu Z. Investigations on the interface of nucleic acid aptamers and binding targets. Vol. 143, Analyst. Royal Society of Chemistry; 2018. p. 5317–38.
30. Tan SY, Acquah C, Sidhu A, Ongkudon CM, Yon LS, Danquah MK. SELEX Modifications and Bioanalytical Techniques for Aptamer–Target Binding Characterization. Vol. 46, Critical Reviews in Analytical Chemistry. 2016.
31. Auiewiriyanukul W, Saburi W, Ota T, Yu J, Kato K, Yao M, et al. Alteration of Substrate Specificity and Transglucosylation Activity of GH13_31 α-Glucosidase from Bacillus sp. AHU2216 through Site-Directed Mutagenesis of Asn258 on β→α Loop 5. Molecules. 2023;28(7).
32. Warfield BM, Anderson PC. Molecular simulations and Markov state modeling reveal the structural diversity and dynamics of a theophylline-binding RNA aptamer in its unbound state. PLoS One. 2017;12(4).
33. Novem Pendidikan Farmasi. 2023;2(1): 35–42.
34. Lawag IL, Yoo O, Lim LY, Hammer K, and Locher C. Optimisation of bee pollen extraction to maximise extractable antioxidant constituents. Antioxidants. 2021; 10(7): 1113.
35. Lukmanto L, Fadhila NIR, Wulandari L, and Puspitasari E. Antioxidant Assay and Total Flavonoid Determination of Ethanolic Extract of Walnut (Canarium indicum L.) Leaves and Its Fractions. Jurnal Ilmu Dasar. 2023; 24 (1) :51.
36. Hasyim SN, Sidik NJ, Chay TC, Rodzali NN, Abdullah SNA, and Muhammad NA. Phytochemical Compounds and Antioxidants Analysis of Clinacanthus nutans Leaf and Stem Extracts. Advances in Science and Technology 2023;127: 3–12.
37. Fawwaz M, Pratama M, Musafira M, Wahab I, Iriani R, Aminah A, Kusuma A T, and Arsul MI. Evaluation of Antioxidant Activity of Vernonia amygdalina Leaves and Its Flavonoid-Phenolic Content. Indonesian Journal of Pharmaceutical Science and Technology. 2023;10(2): 104-10.
38. Susanti N, Mustika A, Khotib J, Muti'ah R, and Rochmanti M. Phytochemical, Metabolite Compound, and Antioxidant Activity of Clinacanthus nutans Leaf Extract from Indonesia. Science and Technology Indonesia. 2023;8(1):38-44.
39. Ramesh MM, Shankar NS, and Venkatappa AH. Driving/ Critical Factors Considered During Extraction to Obtain Bioactive Enriched Extracts. Pharmacognosy Reviews. 2024;18(35): 68-81.Figure, Tables, and Scheme